Passive and active tracking of electrochemical impedance of a drone battery

Hélène Piret, Nicolas Sockeel, Vincent Heiries, Paul-Henri Michel, Marco Ranieri, Viviane Cattin, Nicolas Guillet, Pierre Granjon

European Battery, Hybrid and Fuel Cell Electric Vehicle Congress
Brussels, Belgium, December 1-4, 2015

Passive and active tracking of electrochemical impedance of a drone battery

H. Piret[1a], N.Sockeel[1a], V. Heiries[1a], PH. Michel[1a], M. Ranieri[2a], V. Cattin[1a], N. Guillet[3a], P. Granjon[4a]
[a]*Univ. Grenoble Alpes, F-38054 Grenoble, France*
[1]*CEA, LETI, MINATEC Campus, F-38054 Grenoble, France, helene.piret@cea.fr*
[2]*CEA, LITEN, F-38054 Grenoble, France*
[3]*INES, F-73375 Le Bourget du Lac, France, CEA, LITEN, F-38054 Grenoble, France*
[4]*GIPSA-Lab, F-38000 Grenoble, France*

Abstract

More and more applications rely on batteries, for instance in the field of transport (electrical vehicles), of smart grid, and connected objects. Therefore, the development of battery has become a crucial issue. Unfortunately, a battery is a complex electrochemical system which depends on many parameters and whose performance deteriorates over time. Thus the development of an efficient battery management system (BMS) to avoid damages, to extend lifespan and to optimize the use of batteries is a priority. One way to obtain interesting information representative of the present state of the battery is to estimate its electrochemical impedance. If most of impedance estimation methods rely on the hypothesis of linearity and time invariance, the developed methods intentionally move away from this hypothesis. The goal of the presented work is not only to accurately estimate the impedance over a predetermined frequency range thanks to an algorithm which can be easily implemented in an embedded system but also to be able to track the temporal variations of the impedance. Different methods to estimate impedance both in time and frequency domains are developed and compared. Indeed the aim is first to precisely follow the evolution of the battery impedance in both active and passive identification cases. The evolutionary impedance estimation is then applied to a drone battery. The impedance estimator is used to evaluate the state of charge of the drone battery and other crucial indicators like the remaining flight time thanks to an extended Kalman filter.

Keywords: BMS (battery management system), lithium battery, impedance spectroscopy, state of charge

1 Introduction

More and more applications rely on batteries, for instance in the field of transport (electrical vehicles), of smart grid, of connected objects with for example drones or autonomous devices for home automation. Therefore, the development of battery has become a crucial issue. Unfortunately, a battery is a complex electrochemical system which depends of many parameters and whose performance deteriorates over time. Thus the development of an efficient battery management system (BMS) to avoid damages, to extend lifespan and to optimize the use of batteries, is a priority.

To preserve the integrity of the battery, only non-invasive and non-destructive measurement methods are used, and only external quantities such as the current flowing through the battery, the voltage across its terminals, and its surface temperature [1][2] are measured over time. From these measurements, one way to obtain interesting information representative of the present state of the battery is to measure its electrochem-

ical impedance [3]. This parameter allows to separate resistive and capacitive contributions of a complex system like a battery. The impedance describes its dynamic behavior and is dependent on the history of the battery, its polarization current, its state of charge (SoC), its state of health (SoH) and its internal temperature (T). Consequently, the electrochemical impedance is used in many methods to estimate the internal temperature [4] [5] [6], the SoC [7] [8] [9] and the SoH [9] [10] of the monitored battery.

One of the authoritative methods to measure the impedance is the electrochemical impedance spectroscopy (EIS) [11] [12]. This method belongs to active identification class method [13] and assumes the hypothesis of linearity and time invariance. That is to say in a galvanostatic mode, a single sine wave with low amplitude and fixed frequency is applied as battery current input. The corresponding voltage output variations are measured and used to estimate the unknown impedance at the sine frequency only. To estimate the impedance at several frequencies, the measurement process is repeated. To avoid this sequential implementation, and estimate the impedance for a discrete set of frequencies at one time, a multisine approach can be chosen (the input signal consists of a sum of sines which frequencies correspond to the desired set). Even if the EIS reaches very accurate estimation performance, the method is hard to embed. The generation of sine waves with different frequencies or multisine signals requires advanced electronic generators and so presents an additional cost. Moreover this method gives only one estimate of impedance per measurement. Consequently, each time a new estimated impedance is needed, the whole measurement process must be repeated, strongly limiting the capacity to follow the impedance time evolution that can be significant in case of strong varying operating conditions.

If most of impedance estimation methods rely on the hypothesis of linearity and time invariance like the EIS, the developed methods intentionally move away from this hypothesis. The goal of the presented work is not only to accurately estimate the impedance over a predetermined frequency range thanks to an algorithm which can be easily implemented in an embedded system, but also to be able to track the temporal variations of the impedance. In this paper, different evolutionary impedance estimation methods are first developed and then compared in a stationary case. The time domain method is based on recursive least square (RLS) [14] infinite and finite impulse response filters [15], whereas the frequency method [16] is based on Fourier transform [17] and a local averaging strategy.

The impedance estimation is then applied to a practical application of an autonomous electrical vehicle: a drone. The study is carried out on a DJI Phantom drone and its Lithium-ion polymer battery composed of 3 cells (nominal voltage 3.2 V, nominal capacity of 2.2 Ah) placed in series. To ensure the security of the user, the drone, and its environment, monitoring the battery state during a flight is essential. For such application, the state of the battery changes extremely quickly. Besides the maximum time of a flight is at most around 10 min. Moreover this kind of application presents severe constraints in terms of volume and weight. The embedded calculator should be as light as possible. Indeed the aim is to precisely follow the evolution of the battery impedance during a drone flight. The evolutionary impedance identification is performed in both passive (with the natural current profile during the drone flight) and active (a wideband signal is added) cases. Then this estimated impedance is used to evaluate the SoC of the drone battery and other crucials indicators like remaining flight time and distance thanks to an extended Kalman filter [18] [19] [20].

Section 2 describes the time and frequency domain developed methods to estimate the impedance. In section 3, the different approaches are tested on a real battery in a stationary case and compared to the EIS method. Then in section 4, the frequency domain method is applied to a drone flight in a passive and active identification case. Finally, the evolutionary estimated impedance in the passive case is used with an extended Kalman filter in part 5 to calculate indicators for the drone.

2 Impedance estimation methods

The aim of this section is to develop an evolutionary impedance estimator. The estimator should not only give an accurate estimation but also, it should be able to follow the temporal variations of the impedance.
Different algorithms to precisely estimate and track the impedance are explained in this section. They can be divided into two types:

- the time domain methods
- the frequency domain methods.

2.1 Time domain methods

The time methods correspond to a parametric identification. They are based on recursive least square (RLS) filters. The RLS algorithm [14] is an adaptive filter created to minimize the quadratic error between the measured voltage $u[n]$ and its estimate $\hat{u}$[n] computed from the current $i[n]$. The impulse response coefficients are optimized according to the error by a feedback loop.
This algorithm has the advantage of a quick convergence rate and accuracy however it needs heavy computation. Indeed the computational

cost of the time domain methods is essentially due to the RLS algorithm. The order of the computational cost for one iteration is proportional to n^2 [21] where n is the number of coefficients. Moreover the RLS algoritm needs matrix inversions which complicate the implementation in an embedded system.

Two types of linear filters are tested: infinite impulse response (IIR) [15] filter and finite impulse response (FIR) [15] filter.

2.1.1 Finite impulse response filter

The used FIR filter is based on Eq. (1) and presented in Fig. 1, where $i[n]$ is the input current signal, $\hat{u}[n]$ the estimated output voltage signal, b_k are the feedforward filter coefficients, N is the feedforward filter order.

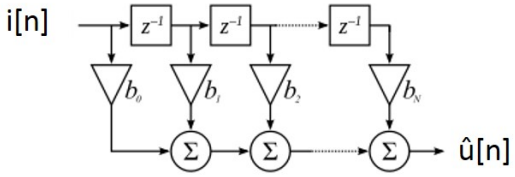

Figure 1: FIR filter

$$\hat{u}[n] = \sum_{k=0}^{N} b_k * i[n-k]. \tag{1}$$

The response of this filter is calculated on a finite number of input values. The FIR filter requires no feedback and so this filter is less sensitive to quantification errors compared to IIR filter. The FIR filter is always a stable filter, its complexity is lower than that of the IIR filter of the same order. Moreover the FIR filter can easily be designed to be linear phase by making the coefficient sequence symmetric.

2.1.2 Infinite impulse response filter

The used IIR filter differs from FIR filter because of the presence of a feedback. Eq. (2) and Fig. 2 describe the equation of the IIR filter, where b_k and a_k are the feedforward and feedback filter coefficients, N and M are the feedforward and feedback filter orders.

$$\hat{u}[n] = \frac{1}{a_0}\left(\sum_{k=0}^{N} b_k * i[n-k] - \sum_{k=1}^{M} a_k * \hat{u}[n-k]\right) \tag{2}$$

The stability of IIR filter depends of the poles position in the complex plan. An IIR filter is more selective than a FIR filter of the same order. Consequently for the same selectivity, an IIR filter need less coefficients than an FIR filter and so need less memory and computations. This explains why the IIR filter is preferred for implementation issues.

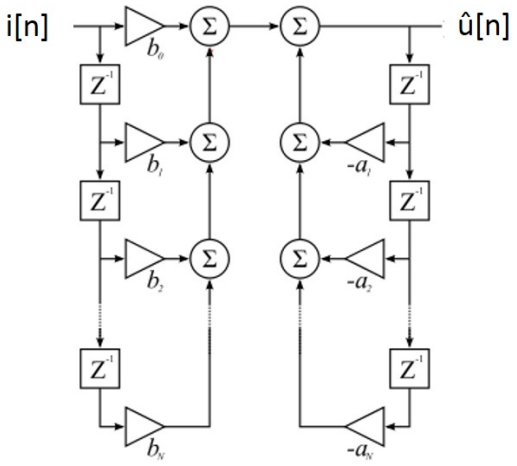

Figure 2: IIR filter

2.2 Frequency domain method

The frequency domain method is a non-parametric identification method based on the Fourier transform and a local averaging strategy.

This method is inspired by the wideband EIS principle. In wideband EIS, the impedance estimator is obtained from a Welch modified periodogram [22]. This estimator is based on a global averaging of all the periodograms of the data. In this paper, the global averaging is replaced by local averaging, which allows to locally estimate the impedance and so to follow its temporal variations.

2.2.1 Linear and time invariant hypothesis

Firstly, variations of the additional current used to estimate the impedance are chosen sufficiently small for the battery to have a linear behavior with respect to these variations. Under this assumption, the battery can be considered as a linear system.

Secondly, parameters on which the battery characteristics depend are assumed to remain constant during the measurement process. Under this assumption, the battery can be considered as a time-invariant system during the measurement time.

Jointly, these two assumptions allow to consider the battery as a linear and time-invariant (LTI) system regarding the additive input-output variations and during the measurement time.
If the battery behaves as a LTI system, its electrochemical impedance $Z(f)$ can be defined by Eq. (3) that is to say by the ratio between the

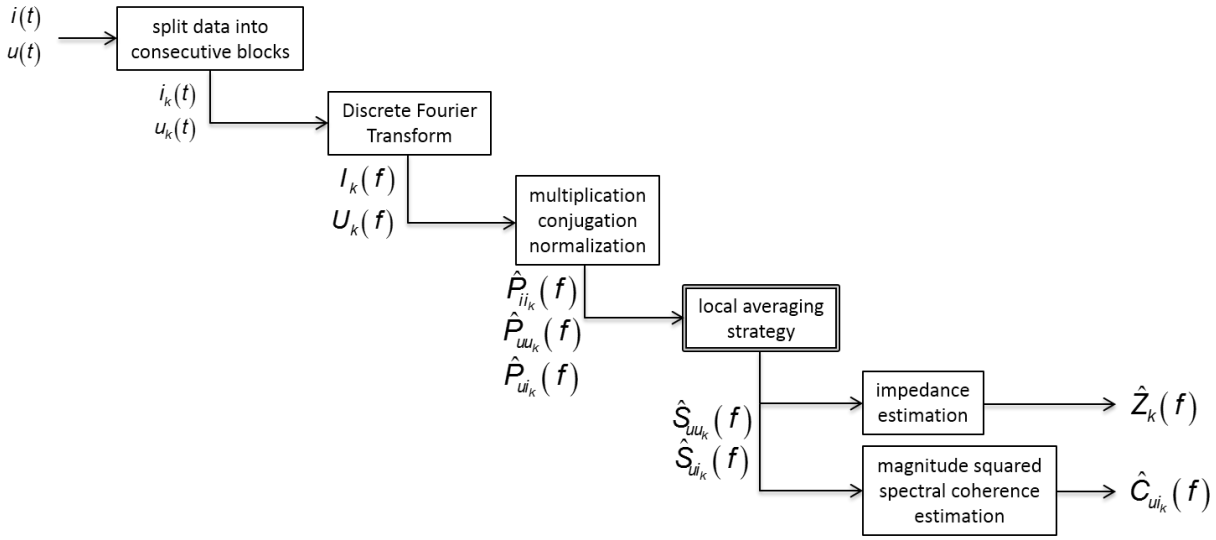

Figure 3: Frequency evolutionary impedance estimation method.

cross power spectral density (CPSD) $S_{ui}(f)$ between voltage and current and the power spectral density (PSD) $S_{ii}(f)$ of the current [17] [23].

$$Z(f) = \frac{S_{ui}(f)}{S_{ii}(f)} \text{ if } S_{ii}(f) \neq 0. \quad (3)$$

2.2.2 Coherence

One way to test if the system can be considered as LTI is to use the notion of squared spectral coherence [24]. This coherence is a statistic quantity that belongs to [0 1]. The squared spectral coherence between the voltage u(t) and the current i(t) is defined in Eq. (4) where $S_{uu}(f)$ is the PSD of the voltage.

$$C_{ui}(f) = \frac{|S_{ui}(f)|^2}{S_{uu}(f)S_{ii}(f)}, \quad (4)$$

$$\text{if } S_{ii}(f) \neq 0, \text{ if } S_{uu}(f) \neq 0.$$

If $|C_{ui}(f)|^2$ tends toward 1 in a given frequency band, the system can be considered as LTI in this frequency band, and so the impedance can be estimated by Eq. (3).
On the contrary, if $|C_{ui}(f)|^2$ tends toward 0, either there is a high level of measurement noise or the system cannot be considered as LTI. In this case, the impedance cannot be estimated by Eq. (4).

2.2.3 Proposed algorithm

In order to estimate $Z(f)$ and $|C_{ui}(f)|^2$, we first estimate the PSD $S_{ii}(f)$,$S_{uu}(f)$ and the CPSD $S_{ui}(f)$.

The data are divided into blocks of same length by using a time window, and their discrete Fourier transform (DFT) is computed by using the fast Fourier transform algorithm.
Fig. 3 presents the different steps of this algorithm. After an initialization step, the impedance and squared spectral coherence estimations are continuously updated using new blocks of data thanks to a recursive equation that implements an exponential averaging strategy using a forgetting factor a.

The value of the forgetting factor controls a trade-off between the convergence time and the final estimation error. The tracking performance is related to the convergence time of the averaging strategy: the smaller the convergence time is, the higher the tracking performance is. On the other hand, the estimation performance is directly related to the amount of residual variations after averaging: the lower the residual variations are, the higher the estimation performance is.

As an example, Eq. (5) and Eq. (6) give the algorithm necessary to recursively estimate the CPSD $S_{ui}(f)$.

$$\hat{P}_{ui_k}(f) = AU_k(f)I_k{}^*(f), \quad (5)$$

$$\hat{S}_{ui_k}(f) = a\hat{S}_{ui_{k-1}}(f) + (1-a)\hat{P}_{ui_k}(f), \quad (6)$$

where A is a normalization factor, * denotes complex conjugation, and $U_k(f)$ ($I_k(f)$ respectively) is the DFT of the k^{th} block of voltage (current respectively) sample, and $a \in [0;1]$ is the forgetting factor. In this equation, the cross periodogram between the k^{th} blocks of voltage and current samples is noted $\hat{P}_{ui_k}(f)$.
Finally the battery impedance is estimated by the

ratio of the estimated CPSD and PSD of current (Eq. (7)). In the same way, the evolutionary coherence estimator corresponds to Eq. (8).

$$\hat{Z}_k(f) = \frac{\hat{S}_{ui_k}(f)}{\hat{S}_{ii_k}(f)}, \text{ if } \hat{S}_{ii_k}(f) \neq 0 \qquad (7)$$

$$\hat{C}_{ui_k}(f) = \frac{|\hat{S}_{ui_k}(f)|^2}{\hat{S}_{uu_k}(f)\hat{S}_{ii_k}(f)}. \qquad (8)$$

$$\text{if } \hat{S}_{ii_k}(f) \neq 0 \text{ if } \hat{S}_{uu_k}(f) \neq 0$$

The implementation cost of the frequency domain method is mainly due to the FFT algorithm which corresponds to a cost that varies in $nfft * log(nfft)$ where $nfft$ is the number of points used to calculate the discrete Fourier transform of current and voltage. That is why the frequency domain method presents a computation cost much lower than time methods. However the frequency domain method needs a little more memory than time domain methods.

Both temporal and frequency domain methods are developed to create an evolutionary impedance estimator. To check the accuracy of each method, they are compared to the reference method (EIS) on a real battery in the next part.

3 Comparison of the methods by an experimental approach in a stationary case

In this part, the three evolutionary impedance estimators are tested on batteries and compared to the EIS reference method. This study is performed on a LiPo battery drone, with a nominal capacity (noted C) of 2.2 Ah.

The three approaches are tested in the stationary active identification case to compare the impedance estimators on the same frequency band than that of the EIS method. The added signal is a pseudo random binary sequence (PRBS) because of its flat spectrum on a chosen frequency band. PRBS signals are more suitable for embedded systems. Indeed, such two-level signals can be generated with very simple electronic circuits.

3.1 Protocol

The battery is placed in an enclosure with controlled temperature of 25 °C. After a complete charge (25 °C, constant current of $\frac{C}{2}$ until 4.2 V, constant voltage during 1h), we discharge the battery at a current of -0.5 A which corresponds to a rate of discharge of $\frac{C}{4.4}$.

We consecutively apply the same block of filtered PRBS block of length 0.25 s, centered again around -0.5 A in order to apply and compare the frequency and time domain methods. This low polarization current allows to minimize the SoC variation during the measurement time.The amplitude of this additive PRBS signal is set to 250 mA, which is sufficiently small for the battery to respect the linear assumption. This block is then filtered thanks to a numeric low-pass filter with a cutoff frequency of 120 Hz to avoid abrupt variations in this additive current. This filtered block is repeated consecutively 36 times, leading to a measurement process with a total duration of 9 s. During this process, the current and the voltage of the battery are synchronously sampled at a rate of 2500 Hz. The studied frequency bandwidth is (20; 90) Hz, due to instrumental constraints.
The estimates obtained by the time-varying wideband frequency algorithm are compared to a known reference impedance called $ZEIS(f)$. This reference is measured through an impedance spectroscopy thanks to a potentiotat VMP3 of Bio-Logic SAS with a booster 20A/20V, associated with the EC-Lab software (signal amplitude of 200 mA, logarithm spacing of 10 measures per decade, 3 measures per frequency). Therefore, once 10 % of SoC is discharged, we first record a classical EIS in a galvanostatic mode at the chosen polarization current.

3.2 Results of time and frequency impedance estimation

An optimization algorithm is applied to fix for the IIR and FIR filters the number of coefficients to have an accurate impedance estimation for several SoC. The forgetting factor of the RLS algorithm is fixed to 1 (the past estimations are considered) and the initial covariance of measurement noise to 10^5. We search the minimal number of coefficients for each filter which ensures an accurate impedance estimation compared to EIS method. There is a couple of numbers of coefficient for which the RLS IIR or FIR filters are optimized. Tab. 1 shows that the IIR filter need less coefficients than the FIR filter.
To compare to the EIS method the temporal impedance estimators are transformed into frequency impedance estimators.The FIR and IIR filters describe a transfer function $H(z)$, the complex-valued frequency response is calculated by evaluating $H(e^{j2*\pi*f})$ at discrete values of the frequency f. The frequency responses of the IIR or FIR filters are calculated and compared to the other methods.
For the frequency method, a forgetting factor of 0.9 is chosen. This value corresponds to a time convergence at 80 % of 3.56 s which is lower than the 9 s of total signal duration.

Fig. 4 highlights the accuracy estimation on a Bode diagram of the three impedance estima-

Table 1: Number of coefficients of FIR and IIR filters for an relative error compared to EIS below 2 %

Filter	FIR	IIR
Number of feedforward coefficients (b_k)	40	6
Number of feedback coefficients (a_k)	0	5

tors at a SoC of 50 %. The time methods are really closer to each other. Although slightly more noisy, the frequency identification for the phase estimate is closer to the reference value than the time domain methods. Indeed all methods follow the trends of EIS method.They are compared to the EIS at several SoC (from SoC 100 % to 50 %).

The root mean square error (averaged on the frequency bandwidth and on 5 values of SoC) on the module and phase are respectively under 1 % and 10 %. The three methods give similarly results for module impedance estimation. They allow to estimate the impedance in the stationary case. The difference between the EIS reference method and the time and frequency methods could result from residual noise, imperfections of the spectral quality of the generated PRBS and also to the battery reaction to the signal excitation.

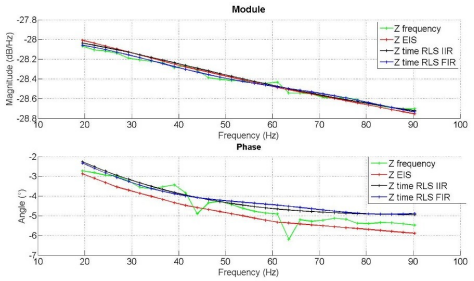

Figure 4: Comparison of impedance estimation between time and frequency methods on a Bode diagram.

The frequency method offers the great advantage of a reduced number of operations. Furthermore the frequency domain method includes the notion of coherence. That is to say, thanks to the high coherence threshold we can ensure the quality of the estimation for each frequency.

The next step is to apply this method in a non-stationary situation. The impedance is then estimated thanks to the frequency domain method in both active and passive identification cases. Indeed the frequency method is applied to estimate the impedance evolution of the drone battery during the flight.

4 Evolutionary impedance estimation during a drone flight

In this part, the frequency domain method is tested in a non-stationary case. The developed method should not only accurately estimate the impedance, but also follow its variations over time.
Two cases are here studied: the passive and active impedance estimations. For the passive identification case, no signal is added at the battery input, only natural profile is used. The impedance estimation is carried out to the natural frequencies which are present in the profile of current.
The active impedance estimation needs to add a signal as the battery input. In this case, the user can choose the frequency band he wants to study.

4.1 Passive impedance estimation

After the validation of the algorithm on a real battery, the frequency method is applied on a battery during a drone flight. The measurement of a drone battery profile (both current and voltage) is recorded in real flight conditions with a multianalyzer recorder (OROS 36, 24-bit resolution) connected to the drone battery with four coaxial cables. Three cables directly acquire the voltage of the three cells composing the drones battery (floating DC connection); one additional cable measures the voltage drop across a $50\ m\Omega$ resistor put in series with the output positive electrode of the battery, in order to acquire an image of the current supplying the drone motors.

Fig. 5 shows the equipment for the drone profile measurement. During the flight the battery surface temperature is monitored and increases only less than $2\ ^{\circ}C$.

Fig. 6 reports an example of the drone natural current profile during a flight, as well as its battery voltage response. The sampling frequency is 2500 Hz. Three steps on the acquired tracks are clearly distinguishable:

- the take-off (first 10 s)
- the flight (middle)
- the landing (end 15 s).

The natural signal of the drone flight excites different frequencies during the flight. Indeed in the passive identification case, natural components of the signals are used, and their frequency band can not control.

The input and output signals are filtered at 50 Hz and its odd multiples to kill off environmental perturbations. The squared spectral coherence defined in Eq. (8) is used to determine the update of impedance estimation. If this spectral quantity exceeds a threshold value of coherence chosen to be close to unity, the system can be considered as LIT and the impedance is estimated at the corresponding frequencies. For these experimental

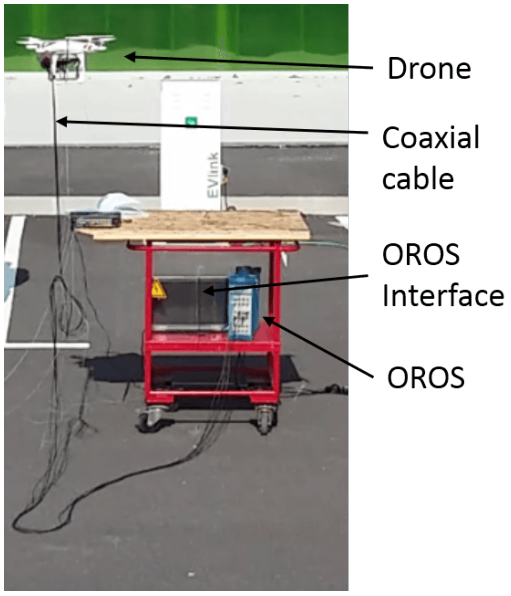

Figure 5: Drone experimentation device.

data, the threshold value of the coherence was set at 0.99. This notion of coherence is a great advantage of the frequency method. Only good impedance estimations (whose coherence exceed the threshold) are retained.

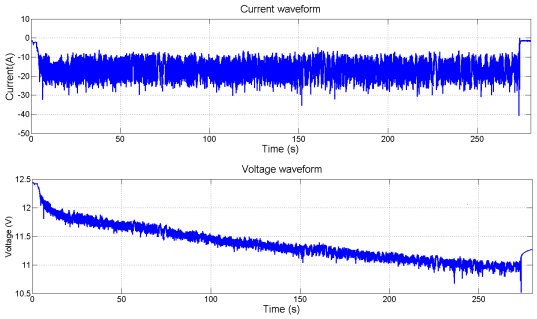

Figure 6: Natural current (top) and voltage (bottom) profile of a drone flight.

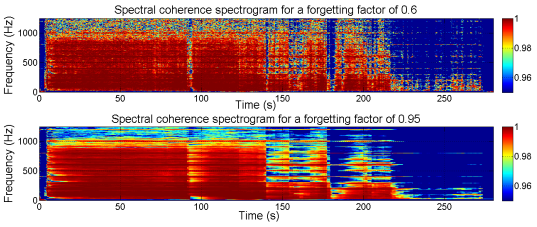

Figure 7: Spectral coherence spectrogram for different forgetting factors (top a=0.6, bottom a=0.95).

The choice of the forgetting factor of the frequency domain method is crucial for the impedance estimation. Fig. reffig:Coherence illustrates the influence of the forgetting factor on the spectral coherence estimator in the passive case. All the coherence value under 0.95 are fixed at 0.95 for a sake of lecture.
For a large forgetting factor, the coherence is sensible to short perturbations (such as before $t < 100\ s$). On the contrary for a low forgetting factor the coherence is more sensitive to long perturbations (such as $t = 180\ s$). This observation is understandable by the fact that a high forgetting factor leads to an important averaging. Moreover the choice of the forgetting factor is directly related to the estimation error after convergence. Therefore a trade-off should be defined.

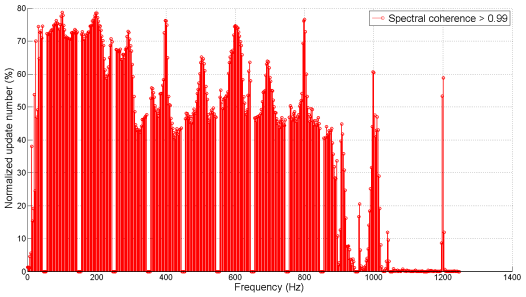

Figure 8: Number of updates according to frequency of the impedance estimation in the passive estimation case.

Fig. 8 shows the update of the impedance estimate as a function of the frequency in a passive case for a forgetting factor of 0.9. In others words the percentage of time for which the spectral coherence exceeds the coherence threshold is given for each frequency. From this figure, we can notice that the natural drone profile is wideband. The impedance is more often estimated for frequencies from 60 to 300 Hz (more than half-time), which allows a regular tracking of the impedance evolution in this frequency band. Thus, the passive case reflects that impedance estimation from natural drone signals is achievable, however, the updated frequency bandwidth depends on the usage profile and is thus not controlled.

Fig. 9 illustrates the tracking of the impedance evolution during a flight. Over the 280 s of flight, the SoC variation corresponds approximatively to 55 %. Between the first (after the convergence time) and last estimations, an evolution of the impedance is clearly visible on both module and phase.

The frequency domain method allows to estimate and track the impedance in passive case. In the context of passive impedance identification, no signal is added, and so no extra electronic circuit is needed, and consequently no weight is added to the drone. Moreover as the natural drone profile is wideband, the impedance could be estimated for applications such as drone monitoring. This is the main reason why the passive impedance estimation is well-suited for an appli-

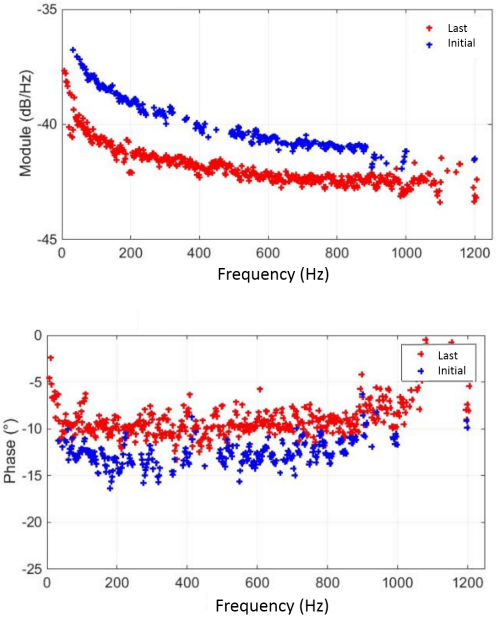

Figure 9: Evolution of impedance estimation (top: module estimation, bottom: phase estimation) on a Bode diagram in the passive case.

cation such as the drone.

4.2 Active impedance estimation

The evolutionary impedance is also tested in the active case. A natural drone profile is used as a current basis. Its current is first normalized to respect the limits of booster (here a booster 20 A/20 V associated with a potentiostat VMP3 of Biologic and Ec-lab software). Then the current signal is filtered at a cutoff frequency of 5 Hz and undersampled at 20 Hz to limit the number of points, in order to be able to record with the potentiostat. The battery is placed in an enclosure with a controlled temperature of 25 °C. After a complete charge (25 °C, constant current of 3 A until 4.2 V, constant voltage during 30 min), we discharge the battery with a modified drone profile. Indeed during the flight part of the profile, the signal is cut. At a polarization current of 15 A, an EIS is applied, then a PRBS block is repeated 79 times (total duration of 20 s) and to finish a second EIS is carried out.

The EIS has an amplitude of 250 mA, and does 2 measurements per frequencies from 10 to 100 Hz with a logarithm spacing of 10 measures by decades. The PRBS block lasts 0.25 s with an amplitude of 250 mA at a sampling frequency of 2500 Hz which corresponds to a frequency bandwidth of (20; 90) Hz.

Fig. 10 shows the input active signal. The drone current for take-off and landing is in blue. In green the two EIS measurements surround the PRBS repeated blocks (red). An EIS corresponds to 2.84 % of SoC variation, whereas the PRBS repeated blocks induce a SoC variation of 3.79 %. The two EIS and the PRBS blocks lead to a SoC variation of approximatively 10 %.

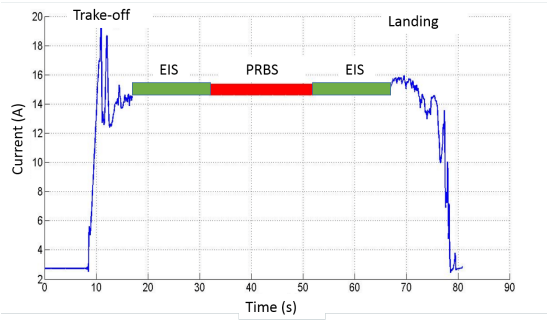

Figure 10: Drone active profile.

The forgetting factor is once again chosen at 0.9 and corresponds to a 80 % convergence time of 3.56 s. Fig. 11 presents the results of the tracking of the evolutionary impedance estimation. The estimated impedance is really surrounded by the two EIS (the first in blue and the second in red). In the course of the discharge, the estimated impedance is at the beginning near the first EIS and then gets closer to the second EIS. So the evolutionary method allows to directly track the impedance variations during the discharge.

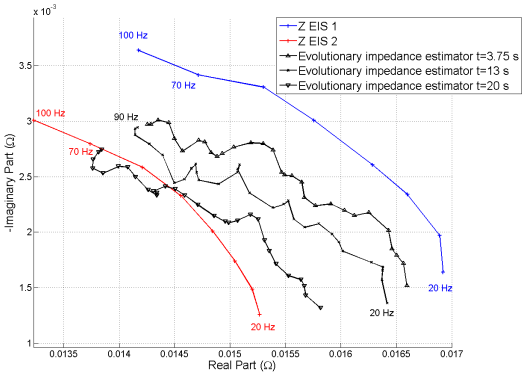

Figure 11: Nyquist diagram of the impedance estimation evolution.

Both passive and active impedance estimations are possible to accurately estimate and track the impedance. Indeed with the evolutionary impedance estimator, we can follow the impedance temporal variations during the drone flight in both cases. This two approaches are not opposite but properly complementary. On the one hand, the passive method only uses the natural profile and so does not need any supplementary signal, so no extra cost and weight. On the other hand the studied frequencies are uncontrolled, they depend only on the profile signal. On the contrary in the active case, the user chooses the added signal and so the studied frequencies, however this operation needs a specific electronic and so leads to additional cost and

weight.
Concerning applications for which specific frequencies should be studied, the active impedance estimation is preferred. If the cost and the weight are essential, and if the natural profile is wideband like for a drone application, passive impedance estimation should be chosen.
The passive estimated impedance is in the next section used in an Extended Kalman filter to estimate the SoC and other drones indicators.

5 Drone indicators from impedance estimates

The impedance can be used to estimate several indicators, like SoC, SoH, and internal temperature. In this part, the evolutionary impedance estimation is used to calculate specific drone indicators (remaining flight time and distance) through the state of charge of the battery (SoC).

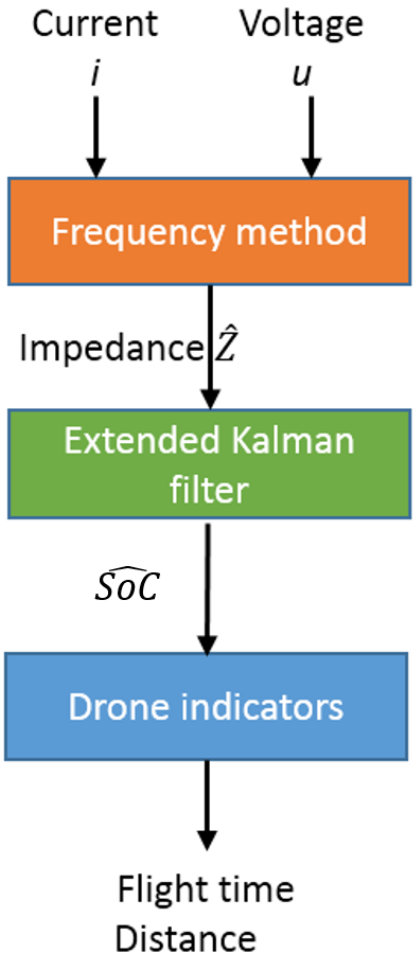

Figure 12: Algorithm to estimate the SoC and the remaining flight time and distance.

Fig. 12 presents the global approach of the algorithm. First the impedance is estimated, by the frequency domain method, then this estimation is used in an extended Kalman filter to continually calculate the SoC. The estimated SoC is then used to estimate the remaining flight time and distance of drone.
This algorithm is applied to a passive frequency impedance identification case. That is to say, the impedance is estimated only with the natural signal already presented in Fig 6. The frequency impedance estimation (complex frequency response) is converted to a discrete-time transfer function thanks to an algorithm based on Levi [25].

5.1 SoC estimation by an extended Kalman filter

5.1.1 Extended Kalman filter

A Kalman filter is used to estimate the state of a dynamic linear system from noisy measurement. The extended Kalman filter (EKF) [26] allows to take into account nonlinear system, such as battery. The EKF presents a bigger computation cost, and the covariance of the error (estimation accuracy) not always converge.
The EKF used in this work, is based on several previous works [18] [19] [20]. For the drone application the state and measurement equations respectively correspond to Eq. (9) and (10).

$$S\hat{o}C_{k+1} = S\hat{o}C_k + \frac{i_k \, \triangle_t}{C_n} + w_k \qquad (9)$$

$$\hat{u}_k = OCV(S\hat{o}C_k) - \hat{Z}_k i_k + v_k \qquad (10)$$

Where
i_k the current
$\triangle_t$ the sampling period
$\hat{u}_k$ the estimated voltage
C_n the nominal capacity of the battery
$OCV(S\hat{o}C)$ open circuit voltage (function of state of charge)
$\hat{Z}_k$ the estimated impedance
w_k state noise
v_k measurement noise.

5.1.2 SoC estimator

The EKF is applied to the natural drone profile to estimate the SoC. Fig. 13 presents the result of SoC estimation. To verify the EKF estimator, a classical coulomb counter method [27] is developed. The error between the two techniques is always under 1 %.
The flight induces 55 % of SoC variation. It is as if a constant current of 16 A was delivered by the battery during 280 s. From the SoC estimation other indicators can be determined.

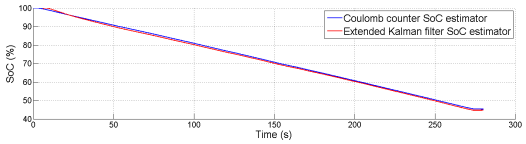

Figure 13: SoC estimation by Coulomb counter and EKF.

5.2 Estimation of remaining flight time and distance

Once the SoC is estimated, the remaining flight time (in min) and distance (in km) can be respectively calculated thanks to Eq. (11) and (12). SoCmin is the minimal limit of SoC that the user chooses (here the SoCmin is fixed to 20 %). The maximal speed of the drone is of 10 $m.s^{-1}$ [28].

$$Flight\,time = \frac{60 * C_n * (\hat{SoC}_{k+1} - SOC_{min})}{100\bar{i}_k} \quad (11)$$

$$Distance = \frac{60 * Flight\,time * speed}{1000} \quad (12)$$

Where $\bar{i}_k$ is the mean current on the last 10 s of the signal duration.

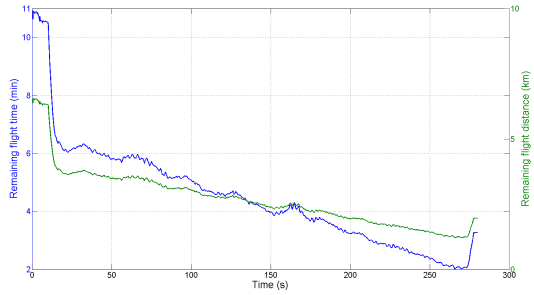

Figure 14: Estimation of remaining flight time and distance over time.

Fig. 14 shows the results of the remaining flight time and distance. After near 4.5 minutes of flight, the remaining flight time is around 2 min left. At this end the drone could only cover approximatively 1 km. The total duration of the flight is around 6.5 min which is less than the order of magnitude given in the datasheet. However for the measurements, the drone is fastened, several coaxial cables and a belt are added for measurements. The drone is so heavier (1.15 kg against a normal weight around 0.8 kg [28]). This overload could explain the gap of remaining flight time with the datasheet. On Fig. (14) the take off and the landing are clearly distinguishable. Indeed before the take-off and after the landing the drone uses less power, which appears on the figure by steps at the beginning and at the end.

From the passive evolutionary impedance estimation, precious indicators for the drone can be calculated thanks to an Extended Kalman filter. This filter calculates the SoC from which remaining flight time and distance are estimated. Over a discharge of more than 50 % of SoC, user can continuously follow the main indicators of the drone.

6 Conclusions

The aim of the presented work is to use an evolutionary impedance method to estimate state indicators such as SoC in real time. Different methods to estimate the impedance both in time and frequency domains are developed and compared. The frequency domain method is based on a discrete Fourier transform as well as an exponential averaging whereas the time domain methods rely on a RLS algorithm associated with an IIR or FIR filter.
The three methods are first tested and compared to EIS in the stationary context. If each method allows an accurate impedance estimation, the frequency domain method presents two decisive advantages. On the one hand, this method is characterized by a low number of operations. On the other hand, the frequency domain method includes the crucial notion of coherence, which can ensure the quality of impedance estimation.
Then evolutionary impedance estimation is carried out to follow impedance evolution of the battery during the drone flight. The developed frequency method can be used both in the passive and active contexts. This two approaches are not opposite but complementary. The active methods need to generate an additional signal, but in this case the frequency bandwidth can be chosen by the user. The passive case does not need any signal generation, only the natural profile is used, however, the studied frequencies only depend on the profile. According to the application one approach should be preferred. For example if specific frequencies should be studied active method should be chosen. If like in the drone case, the weight and the cost are crucial, and if in addition the natural profile is frequency-rich, then the passive method is more appropriate.
The impedance is subsequently used to estimate the SoC, but it could also be used to estimate other indicators such as the SoH or the internal temperature. In this paper thanks to the estimated impedance, crucial parameters for the drone (remaining flight time and distance) are continuously estimated with an extended Kalman filter.
As a further step, the SoH and the internal temperature will also be studied. Moreover this method will be implemented into an embedded system (a drone) and this demonstrator will be used to estimate its battery parameters in real time.

References

[1] D. Andrea. *Battery Management Systems for large Lithium Ion Battery Packs*, 2010.

[2] M. Coleman, C. K. Lee, C. Zhu and W. Hurley, *State-of-charge detertmination from EMF voltage estimation: Using impedance, terminal voltage, and current for lead-acid and lithium ion batterie*, IEEE Transactions on industrial electronics, 54(2007), 2550-2557.

[3] D. Howey, V. Yufit, G. Mitcheson, G. Offer and N. Brandon, *Impedance measurement for advanced battery management system*, in EVS27 Internationale Battery, Hybrid and Fuel Cell Vehicle Symposium, 2013.

[4] J. Zhu, Z. Sun, X. Wei and H. Dai, *A new lithium battery internal temprature in-line estimate based on electrochemical impedance spectroscopy measurment*, Journal of Power Sources, 274(2015),990-1004.

[5] R. Richardson, P. Ireland and D. Howey, *Battery internal temperature estimation by combined impedance and surface temperature measurement*, Journal of Power Sources, 265(2014),254-261.

[6] J.-P. Schmidt, S. Arnold, A. Loges, D. Werner, T. Wetzel and E. Ivers-Tiffe *Measurement of the internal cell temperature via impedance: Evalulation and application of a new method*, Journal of Power Sources, 243(2013),1110-1172.

[7] K. Bundy, M. Karlsson, G. Lindbergh and A. Lundqviste *An electrochemical impedance spectroscopy method for prediction of the state of charge of a nickel-metal hydride battery at open circuit and during discharge*, Journal of Power Sources, 72(1998),118-125.

[8] S. Rodrigues, N. Munichandraiah and A. Shukla *A review of state-of-charge indication of batteries by means of a.c. impedance measurements*, Journal of Power Sources, 87(2000),12-20.

[9] H. Blanke, O. Bohlen, S. Buller, R. Doncker, B. Fricke, A. Hammounche, D. Linzen, M. Thele and D. Sauer *Impedance measurements on lead acid batteies for state-of-charge and state-of-health and cranking capability prognosis in electric and hybrid electrical vehicules*, Journal of Power Sources, 144(2005),418-425.

[10] U. Troltzsch, O. Kanoun and H. Trankler *Characterizing aging effects of lithium batteriesby impedance spectrocospy*, Electrochemica Acta, 51(2006),1664-1672.

[11] E. Barsoukov and J. R. Macdonald, *Impedance Spectroscopy - Theory, Experiment, and Applications*, Wiley, 2005.

[12] M. Orazem and B. Tribolle *Electrochemical Impedance Spectroscopy*, Prentice Hall, 2011.

[13] L. Ljung *System Identification - Theory for the User*, Prentice Hall, 1999.

[14] M.H. Hayes *Statistical Digital Signal Processing and Modeling*, Wiley, 1996.

[15] M. Najim *Digital filters Design for Signal and Image Processing Digital Signal*, Wiley-ISTE, 2006.

[16] R. Al-Nazer, V. Cattin and P. Granjon *Broadband identification of battery electrical impedance for HEVs*, IEEE Transactions on Vehicular Technology, 62(2013),2896-2905.

[17] R. Pintelon and J. Schoukens *System Identification - a Frequency Domain Approach*, Wiley, 2012.

[18] G. Plett *Extended Kalman filtering for battery management systems of LiPB-based HEV battery packspart 1: Background*, Journal of Power Sources, 134(2004),252-261.

[19] G. Plett *Extended Kalman filtering for battery management systems of LiPB-based HEV battery packspart 2: Modeling and identification*, Journal of Power Sources, 134(2004),262-276.

[20] G. Plett *Extended Kalman filtering for battery management systems of LiPB-based HEV battery packspart 3: Parameter estimation*, Journal of Power Sources, 134(2004),277-292.

[21] A. Sayed *Fundementals of Adaptive Filtering*, John Wiley & Sons, 2003.

[22] P. Welch *The Use of Fast Fourier Transform for the Estimation of Power Spectra: A Method Based on Time Averaging Over Short, Modified Periodograms*, IEEE Trans. on Audio Electroacoustics, 15(1967),70-73.

[23] K. Shin and J. Hammond *Fundamentals of Signal Processing for Sound and Vibration Engineers*, Wiley, 2008.

[24] J. S. Bendat and A. G. Piersol *Random Data - Analysis and Measurement Procedures, 4 ed.*, Wiley, 2010.

[25] E. Levi *Complex-Curve Fitting*, IEEE Trans. on Automatic Control, AC-4(1959),37-44.

[26] B. D. O. Anderson and J. B. Moore *Optimal Filtering*, Prentice-Hall, 1979.

[27] K. Ng, C. Moo, Y. Chen and Y. Hsieh *Enhanced coulomb counting method for estimating state-of-charge and state-of-health of lithium-ion batteries*, Journal of Applied Energy, 86(2009),1506-1511.

[28] Phantom *Manuel de dmarrage rapide, Drone DJI*,2013.

Authors

H. Piret received the Engineering degree in electronics from National Graduate School of Engineering of Caen (ENSICAEN), France, in 2013. She is currently a PhD student in signal processing on impedance measurement (application to battery) at Atomic Energy and Alternative Energies Commission, Grenoble, France.

N. Sockeel, PhD student at the Electrical and Computering Engineering department of Mississippi State University, Mississippi, United State. He obtained a M.Sc Degree in Conventional and Sustainable Energy at EPF, a French Graduate School of Engineering.

V. Heiries is graduated from ENAC (Ecole Nationale de lAviation Civile) and holds a PhD in signal processing and digital communications. He has worked several years in the field of navigation systems (GNSS, UWB). His activities in the CEA are now mainly focused on signal processing applied to battery monitoring.

PH. Michel is graduated in signal processing from ENSE3, an engineering school of Grenoble Institute of Technology. He currently works as a research engineer in the fields of system monitoring at Atomic Energy and Alternative Energies Commission, Grenoble, France.

M. Ranieri obtained is degree in Electronic Engineering in 2005 at the University of Bologna. He has worked in CEA-Grenoble since 2008, focusing on BMS systems, embedded electronics for the Smart Cell as well as on monitoring systems for Fuel Cell. He coordinates the participation of the CEA to one European project about integrated components for electric vehicles.

V. Cattin received the Ph.D. degree from Grenoble Institute of Technology (INPG), Grenoble, France, in 1998. She is currently a Research Engineer in the fields of applied signal processing for sensors systems with Atomic Energy and Alternative Energies Commission, Grenoble, France.

N. Guillet received its PhD in Physical Chemistry from the Mining School of St Etienne (ENSMSE), France in 2001. After 2 years of post-doctoral position at INRS of Varennes (Canada) he joined the CEA/Liten as research engineer and is expert for CEA in electrochemistry and electrochemical storage of energy (fuel cell, batteries).

P. Granjon received the Ph.D. degree from the Grenoble Institute of Technology, France in 2000. He joined the Laboratoire des Images et des Signaux (LIS) in 2002 and the Gipsa-lab at INPG in 2007, where he holds a position as associate professor. His current research is mainly focused on signal processing methods for electrical systems monitoring, such as fault detection and diagnosis in power networks, rotating machinery and batteries.